Electrochemical performance of controlled porosity resorcinol/formaldehyde based carbons as electrode materials for supercapacitor applications

Abbas, Qaisar; Mirzaeian, Mojtaba; Ogwu, Abraham A.

Published in:
International Journal of Hydrogen Energy

DOI:
10.1016/j.ijhydene.2017.04.078

E-pub ahead of print: 08/05/2017

Document Version
Peer reviewed version

Electrochemical performance of controlled porosity resorcinol /formaldehyde based carbons as electrode materials for supercapacitor applications

Qaisar Abbas, Mojtaba Mirzaeian[*] and Abraham A Ogwu

School of Engineering and Computing, University of the West of Scotland, Paisley PA1 2BE, United Kingdom.

Corresponding author e-mail address: mojtaba.mirzaeian@uws.ac.uk

Abstract

Controlled porosity carbons aerogels were synthesized by sol-gel polycondensation of resorcinol (R) and formaldehyde (F) using sodium-carbonate as the catalyst (C). The Effect of variation of R/C ratio and carbonization temperature on the porous structure of resultant gels and carbons was investigated by characterizing the porous structure of the materials using nitrogen adsorption-desorption measurements at 77 K. It was shown that carbons with surface areas ranging between 537 − 687 m^2g^{-1} and average pore size in the range of 1.80 − 4.62 nm can be produced when controlling the resorcinol to catalyst (R/C) molar ratio between 100 − 500 and carbonization temperature in the range of 800 − 1000 ºC.

The resultant polymeric carbons were used as the electroactive material for the fabrication of electrodes for electrochemical cells. Contact angle measurements were performed to study the wettability of the electrodes using 6 M KOH as the probing liquid. The contact angles were in the range of 106 − 125 degrees indicating the carbon based electrodes are hydrophobic in nature and no significant change in contact angles was observed with the change in R/C ratio.

XRD patterns of the carbon electrodes show a typical broad peak at 2θ of about 23 indicating a disordered structure corresponding to the amorphous nature of the materials as expected for polymeric based hard carbons with crosslinked structure. These results are in line with Raman spectra of carbons which indicate two peaks in 1590 cm^{-1} and 1340 cm^{-1} wavenumber.

The electrochemical performance of the electrodes was investigated by cyclic voltammetry (CV) and electrochemical impedance spectroscopy (EIS) measurements. The CV results showed that high specific capacitance of 136 Fg^{-1} can be achieved for the carbon with average pore diameter of 1.80 nm at a scan rate of 5 mVs^{-1} when using 6M KOH as the electrolyte. Electrochemical impedance (EIS) measurements also revealed that the capacitance of the cell deteriorates with increase in pore size of the carbon probably due to pore flooding by the electrolyte. The results of this study show the applicability of these carbons as potential electrode materials for supercapacitor applications.

Keywords

Porosity; Specific surface area; Specific capacitance; Supercapacitors; Electrochemical measurements

Introduction

As the world's energy forecast shows, the global energy demand is going to be doubled in next 50 years [1]. With increase in energy requirement of upcoming systems and associated concerns on the depletion of fossil fuels and their environmental related effects in the planet, deployment of renewable energy sources such as wind, wave and solar will play a key role in our future energy demands. Study suggests that at the end of 2013 global renewable energy generation capacity reached 1560 GW, almost double than the estimated figure of 895 GW at the start of the year 2004 [2]. The capacity of global renewable energy generation is currently at 1707 GW [3] indicating a significant increase in the contribution of renewable energy resources to our energy demands. However due to the unpredictable and intermittent nature of these energy resources and as the security of the supply is crucial in any energy system, employment of the renewables is only possible when effective energy storage technologies commensurate with each application are developed. Batteries, fuel cells and supercapacitors are in the forefront of energy storage technologies. However due to their energy storing and releasing capabilities in limited time scales, they cannot respond to all energy requirements of future devices. Batteries and fuel cells are only effective for the storage and delivery of energy at slow rates over a long period of time [4, 5]. While in high power applications when a surge of energy in a short time is required, storage technologies such as electrochemical capacitors become imperative to respond to the short term fluctuations in energy outputs and improve the quality of the energy supply. Properties such as rapid charge/ discharge, exceptionally high capacitance retention and long cycle life make electrochemical capacitors as ideal candidates to complement other primary storage devices when a wide spectrum of energy and power is required [6, 7]. The performance of electrochemical capacitors depends on the type of electrode and electrolyte materials used in their manufacture.

Due to its chemical inertness, exceptionally high specific surface area, electrical conductivity and tailored pore size, carbon is the most widely used electroactive material for the fabrication of electrodes in supercapacitor industry [8-10].

Polymeric carbons obtained from the pyrolysis of resorcinol-formaldehyde (RF) aerogels have been used as active material for various energy storage devices due to their desirable properties such as high porosities (>80%), high specific surface area (700-2600 m^2g^{-1}) , pore

volume (0.179 -2.195cm^3g^{-1}) and exceptional conductivity as a result of their three dimensional cross-linked structure. Their properties and particularly their porous structure can be tuned by the control of synthesis parameters during gel preparation and also through the control of processing conditions during carbonization and activation processes [11-13].

In this work, we have synthesized RF based carbon aerogels with controlled porosity by controlling the resorcinol to catalyst molar ratio (R/C) during the preparation of the gel precursor and also controlling the carbonization temperature during the production of carbons. The effect of porous structure of the resultant carbons when used as the electrode material with 6M KOH solution as the electrolyte in an electrochemical cell on the capacitance of the device is investigated by cyclic voltammetry (CV) measurements. Electrochemical impedance (EIS) measurements are also carried out to elucidate the effect of electrode's porosity and electrode/electrolyte interfacial resistances on the performance of the electrochemical cell.

Experimental

Synthesis of RF gels

Resorcinol (R) formaldehyde (F) aerogels were prepared by polycondensation reaction between resorcinol and formaldehyde according to the procedure explained elsewhere [13, 14]. Predetermined amount of resorcinol and sodium carbonate as catalyst (C) were mixed in distilled water (W) under vigorous stirring for 45 min. Formaldehyde was added and the stirring was continued for another 45 min at room temperature. The resorcinol to formaldehyde molar ratio (R/F) and the ratio of the amount of resorcinol to the amount of water used (R/W) in gml^{-1} were kept constant at 0.5 and 0.1 respectively whereas the resorcinol to catalyst molar ratio (R/C) was varied in the rage of 100 to 500. The homogenous solutions were transferred into the sealed glass vails to prevent the evaporation of water during the gelation process and placed in the oven where temperature was controlled first at 25 ºC for 24 h to initiate gelation process followed by increasing the it to 60 ºC for 72 h and further increase to 80 ºC for 48 h for the completion of the gelation process. This long gelation time ensures a well-developed three dimensional gel structure. The resultant dark opaque aqua-gels were broken into small pieces and immersed in acetone for 4 days for solvent exchange to extract water from the porous structure of hydrogels completely prior to their drying. The gels then were dried under vacuum at 5 mbar and 40 ºC for 4 days to completely remove acetone from the internal pores of the gel without any shrinkage [14].

Carbonization of RF aerogels

The dried RF aerogels were carbonized at different temperatures to investigate the effect of pyrolysis conditions on the porous structure of carbon aerogels. A sample of gel (≈ 3g) in a ceramic boat was placed in the middle of a tubular furnace and purged with Ar at room temperature for 30 min prior to the pyrolysis. The temperature was increased at a rate of 5 ºC min^{-1} to 150 ºC and maintained for 30 min. The temperature was further increased to 450 ºC at a rate of 5 ºC min^{-1} and held for 30 min. Finally it was increased to 800 ºC at 10 ºC min^{-1} and the sample was kept at this temperature for 3h before cooling it down to the room temperature. The entire process was performed under Ar flowing at rate of 240 ml min^{-1}.

Electrode preparation

Electrodes for electrochemical measurements were prepared using carbon in the form of well grinded powder. Approximately 80 wt% active carbon material, 10 wt% Cabot carbon black XC72 as conductivity enhancer and 10 wt% Kynar 2801 as binder were used for the fabrication of electrodes. The electrode components were mixed with acetone for 2 hours to form a paste. The paste then was rolled into sheets with the wet film thickness of 250 µm using a doctor blade. Circular discs with diameter of 1.33 cm were then punched out from the films and dried overnight in a vacuum oven at 85 ºC resulting in a dry thickness for the electrodes in the range of 10 – 20 micrometres.

Cell construction

Sandwich type symmetric capacitor cells were constructed with a pair of carbon electrodes cast on aluminium foil using glass microfiber as the separator as shown in Figure 1.

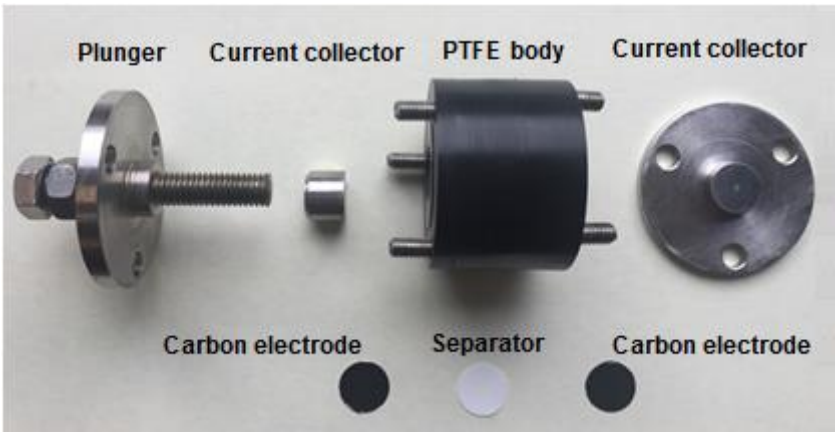

Figure 1 Schematic of the electrochemical capacitor test cell.

The test cells consisted of an insulating Polytetrafluoroethylene (PTFE) body that is resistant to corrosion by the electrolytes. The current collectors are stainless steel with the upper

current collector being controlled by a stainless steel plunger which is sealed with a PTFE screw seal. The plunger moved independently from the current collector to prevent damage to the electrodes when tightened. A 6M KOH solution used as the electrolyte was added to the separator located between two electrodes and the cell was sealed and placed under vacuum for 20 min to ensure the electrolyte penetration in porous structure of the electrodes prior to the electrochemical measurements.

Electrochemical measurements

Electrochemical measurements were conducted using a Voltalab 40 radiometer analytical potentiostat. The cell was kept under open circuit for 15 minutes to stabilize prior to all electrochemical measurements. Cyclic voltammetry (CV) measurements were used for the capacitance calculations with a voltage range between 0.5 and 1 V at scan rates of 5, 10, and 15 mVs^{-1}. Electro-chemical impedance spectroscopy (EIS) was also performed at the AC voltage amplitude of 10 mV and the frequency range of 100 KHz to 5 Hz with number of frequencies (per decade) of 5.

Physical characterization of the materials

The porous structure of RF aerogels and carbon was characterized by a Tri-Star adsorption analyser (Micromeritics). The samples were evacuated in a vacuum oven at 80 ºC at 5 mbar for 24 h and then they were further purged in a nitrogen flow at elevated temperatures (80 ºC for gels samples and 300 ºC for carbons) in a Flowprep system (Micrometrics) prior to the adsorption/desorption measurements. BET method was used for surface area measurements, t-plot method was used for micropore analysis, and BJH method using adsorption branch of the isotherms was used to calculate pore size distributions. The total pore volume was determined from the adsorbed volume of nitrogen at saturation pressure ($P/P_0 = 0.99$) [15].

Contact angle measurements were carried out using a CAM 200 goniometer system manufactured by KSV Ltd based on video captured images and automatic image analysis using CAM software. 6M KOH was used as the probe liquid for contact angle measurements.

Raman spectroscopy was carried out on an “In via Raman microscope (Renishaw, UK)” with 514.5 nm diode laser excitation in the range of 1000 cm^{-1} and 3000 cm^{-1} to evaluate the vibrational properties of the electroactive material.

X-ray diffraction (XRD) was performed using a SIEMENS - D5000 X-ray diffractometer with the voltage and current kept at 40 kV and 30 mA respectively to analyse the morphological structure of carbonised aerogels.

Results and Discussions:

BET analysis of the samples

Figure 2 shows the N_2 adsorption-desorption isotherms of RF gels. The RF aerogels are named as RFx where x is the R/C ratio used during the synthesis of the gel. All isotherms show a type IV isotherm with H2-type hysteresis loop which is the indicative of well-developed micro and messoporisity within the materials [16]. The sample with the R/C ratio of 100 shows a microporous structure with the absence of the hysteresis loop. For samples with the R/C ratio between 200 – 400 steep increase in adsorbed volume in lower P/P_0 indicates the presence of microporosity followed by a hysteresis loop which is indicative of messoporisity within the samples. The hysteresis loops become wider at higher P/P_0 for samples with higher R/C ratios particularly for samples with R/C ratios of 400 and 500 indicating well-developed mesoporous structures [17].This indicates the development of mesoporosity and formation of larger mesopores during gelation process at higher R/C ratios.

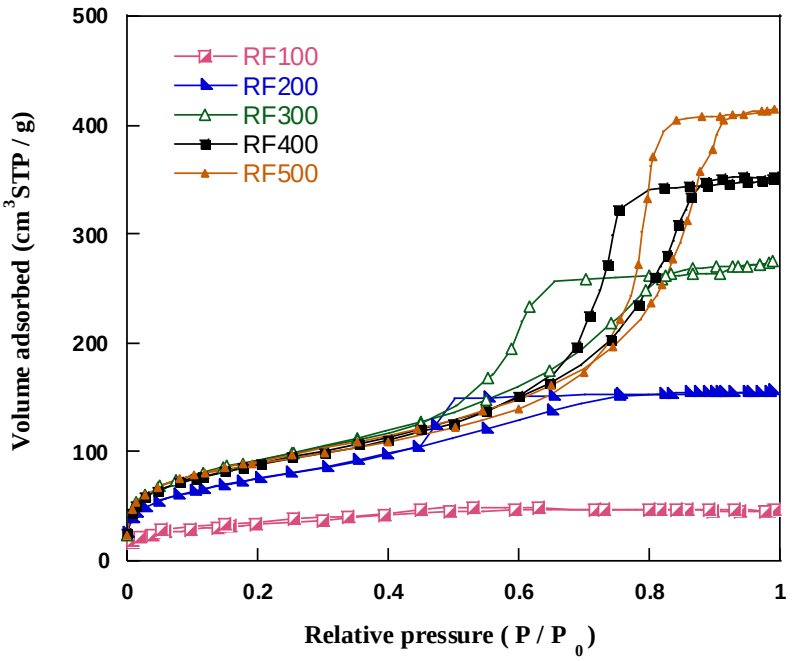

Figure 2 N_2 adsorption–desorption isotherms of RF aerogels with different R/C ratios.

Pore size distribution (PSD) of the RF gels is shown in Figure 3. The average pore size considered as the BJH adsorption average pore width (4V/A) is an indication of the average of all pores within the material. It can be seen that the average pore size increases with increase in R/C ratio. Sample with R/C ratio of 100 shows a narrow PSD with the maxima around 2 nm. Increasing the R/C ratio to 200 increases the pore diameter above 3 nm. For the sample with R/C ratio of 500, PSD curves are even wider and pore diameter is increased to nearly 8 nm. This in mainly due to the formation of larger clusters at higher R/C ratios during the gelation process which result in inter-particle paths acting as the pores with in the structure of the final gels [13].

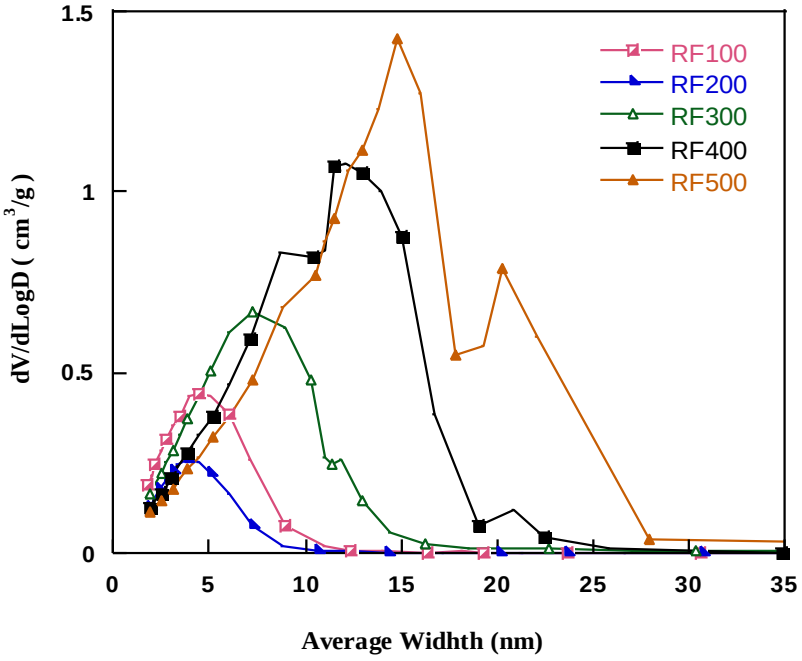

Figure 3 Pore size distribution of RF aerogels with different R/C ratios.

Table 1 summarizes the porosity parameters of the gel samples. As seen the mesoporosity of the samples increases with the increase in R/C ratio and this behaviour is well consistent with pore size distribution where pore size increases from 2.6 nm to 7.97 nm with the variation of R/C ratio between 100 and 500. According to IUPAC notation, microporous materials have pore diameters of less than 2 nm and macroporous materials have pore diameters of greater than 50 nm; the mesoporous category thus lies in the middle [18]. This indicates that with increasing R/C ratio a range of RF gels with microporous to mesoporous structure can be developed.

Table 1 Porosity parameters of aerogel samples with different R/C ratio.

Sample	R/C	S_{BET} (m^2g^{-1})	V_{total} (cm^3g^{-1})	V_{micro} (cm^3g^{-1})	V_{messo} (cm^3g^{-1})	V_{micro} %	V_{meso} %	D_{ave} (nm)
RF100	100	117	0.0714	0.0058	0.0656	8	92	2.60
RF200	200	256	0.2406	0.0011	0.2296	5	95	3.40
RF300	300	327	0.4282	0.0028	0.4254	1	99	5.20
RF400	400	313	0.5624	0.0052	0.5572	1	99	6.78
RF 500	500	322	0.6409	0.0075	0.6334	1	99	7.97

Since the chemical composition of all gels is analogous, the RF200 gel was selected as a typical sample to find out the effect of carbonisation temperature on the porous structure of the resultant carbons and the temperature at which the optimum pore size and surface area for the carbons are obtained. This temperature will be used for the carbonisation of all gels to prepare carbons with different porous structures obtained from the gels with different R/C ratios afterward. All carbons aerogels are named as RFCx – y where x is the R/C ratio used during the synthesis of the gel precursor and y is the temperature in ºC used for the carbonization of the gels.

Figure 4 shows N_2 adsorption-desorption isotherms for the gel with R/C ratio of 200 and the carbon aerogels produced form this gel at different temperatures.

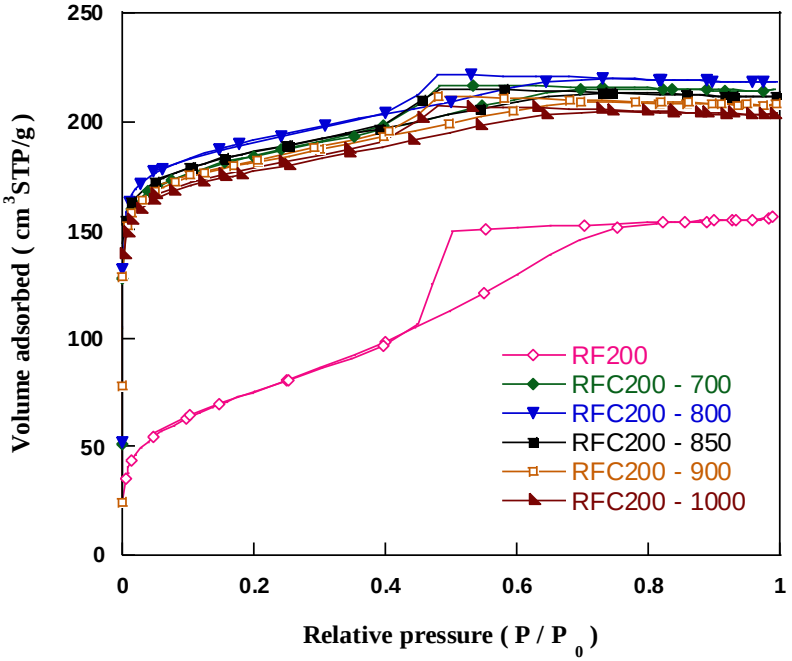

Figure 4 N_2 adsorption–desorption isotherms for RF200 gel and carbon aerogels produced at different temperatures.

It can be observed that carbonization results in a drastic increase in the specific surface area for all the carbons. A significant increase in volume adsorbed at lower $P/P_0 < 0.2$ shows the development of microporosity whereas hysteresis loops at relative pressure P/P_0 between 0.4 – 1.0 indicates the presence of mesoporosity in the samples [19]. A decrease in adsorbed volume at temperatures above 800 ºC is explained as the result of the collapse of the pore structure at high temperatures [20].

Figure 5 shows the pore size distribution curves for carbon aerogels obtained at different temperatures. The PSD curves show a bimodal trend for carbons indicating the presence of both micropores cantered around 2 nm and small mesopores cantered around 4 nm within their structure [18, 21]. This is mainly due to the opening of closed micropores during the pyrolysis process as the result of the release of volatile components at elevated temperatures. This has been evidenced by thermogravimetric analysis (TGA) of the RF gels at temperatures above 450 ºC in previous works [13]. It can be seen also that due to the structural change during the carbonisation process the level of mesoporosity in the resultant carbons decreases. It is believed that the carbonisation opens micropores and at the same time decreases the level of mesoporosity with gradual collapse of the structure at elevated temperatures [13].

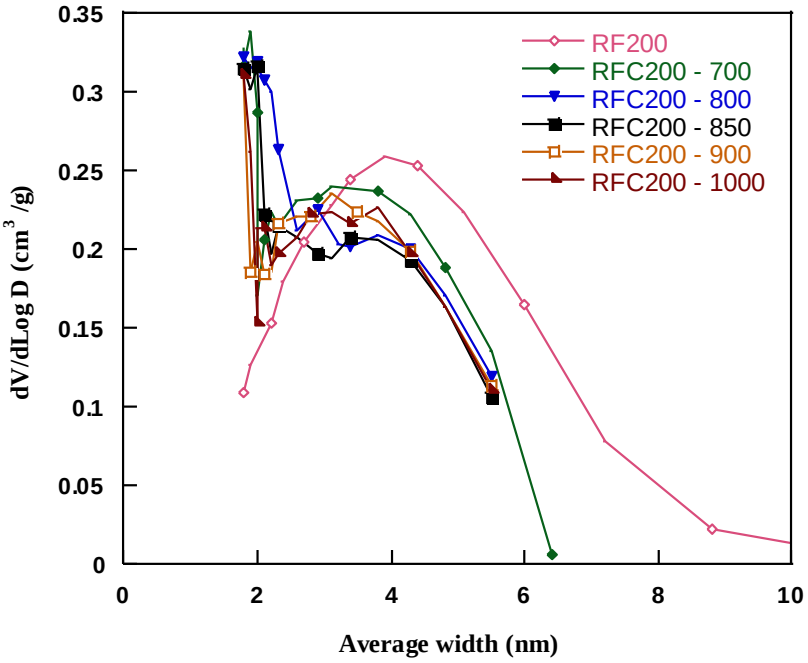

Figure 5 Pore size distribution of carbon aerogels produced at different temperatures.

Table 2 shows the porosity parameters of the RF 200 aerogel and RFC 200 carbon aerogels produced at different temperatures. The specific surface area increases due to carbonization

of the gel samples with highest surface area obtained at 800 ºC. However for carbons produced at temperatures above 800 ºC a gradual decrease in surface area is observed. Temperature of 800 ºC is the most effective for the development of the pore structure of the gel and increasing the carbonization temperature beyond this temperature results in the collapse of the carbon structure and decrease in the porosity. The temperature of 800 ºC is considered as the optimum temperature for the preparation of carbon aerogels with different R/C ratio.

Table 2 Porosity parameters of the RF 200 aerogel and RFC 200 carbon aerogels produced at different temperatures.

Sample	S_{BET} (m^2g^{-1})	V_{total} (cm^3g^{-1})	V_{micro} (cm^3g^{-1})	V_{meso} (cm^3g^{-1})	V_{micro} %	V_{meso} %	D_{ave} (nm)
RF 200	256	0.2406	0.0011	0.2296	5	95	3.80
RFC 200- 700 ºC	616	0.3321	0.2058	0.1263	38	62	2.94
RFC 200- 800 ºC	638	0.3373	0.2093	0.1280	62	38	2.87
RFC 200- 850 ºC	617	0.3269	0.2088	0.1181	64	36	2.90
RFC 200- 900 ºC	604	0.3214	0.2107	0.1107	66	34	2.96
RFC 200-1000 ºC	586	0.3149	0.2052	0.1097	65	35	2.93

Figure 6 shows N_2 adsorption–desorption isotherms of carbons prepared from aerogels with different R/C ratios at 800 ºC. Nitrogen adsorption-desorption isotherm for RFC 100 (R/C = 100) shows a microporous structure with quick N_2 intake at very low pressure due to of micro pore filling at low P/P_0 [22, 23]. For the RFC 200 sample the initial region of $P/P_0 < 0.1$ represents microporosity whereas for P/P_0 in the range of 0.4 – 0.8 shows the presence of messoporisity as the hysteresis loop. The hysteresis loop shifts toward higher P/P_0 with the increase in R/C ratio as a result of larger mesopores in the carbon structure.

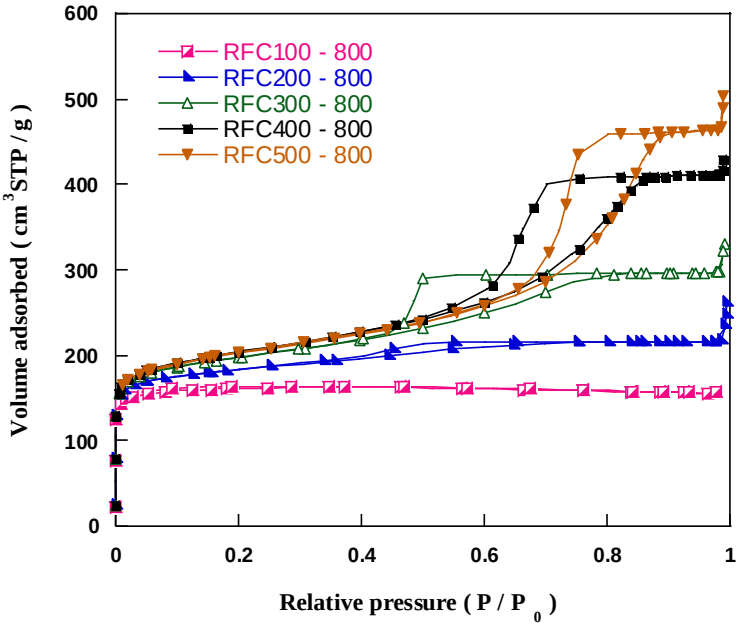

Figure 6 N_2 adsorption–desorption isotherms of carbon aerogels with different R/C ratios produced at 800 ºC.

The PSD curves for the carbon samples with different R/C ratios produced at 800 ºC are shown in Figure 7. RFC 100 sample shows a peak around the pore diameter of 2 nm and the PSD curves moves towards larger dimeter pores with the increase of R/C ratio with a peak centred around 15 nm for RFC 500 sample.

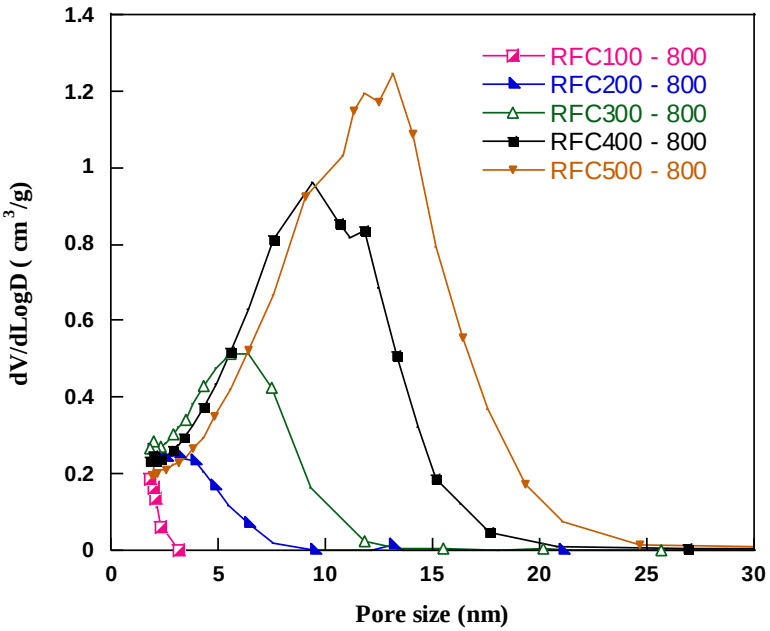

Figure 7 Pore size distribution of carbon aerogels with different R/C ratios.

The porosity parameters carbon samples with different R/C ratios produced at 800 ºC are given in Table 3. These results show increase in mesoporisity with the increase in R/C ratio.

Table 3 porous parameters of carbon samples at 800 ºC (effect of R/C ratio)

Sample	S_{BET} (m^2g^{-1})	V_{total} (cm^3g^{-1})	V_{micro} (cm^3g^{-1})	V_{messo} (cm^3g^{-1})	V_{micro} %	V_{meso} %	D_{ave} (nm)
RFC100	537	0.2420	0.2167	0.0253	90	10	1.80
RFC200	613	0.4085	0.2031	0.2054	50	50	2.67
RFC300	633	0.5113	0.1914	0.3199	37	63	3.08
RFC400	687	0.6675	0.1859	0.4816	28	72	3.89
RFC500	673	0.7778	0.1876	0.5902	24	76	4.62

The sample with R/C ratio of 100 possesses 90% micropores and 10% mesopores. As the R/C increase from 100 to 500, the total pore volume of the carbon increases from 0.24 to 0.78 cm^3g^{-1} and the average pore size also increases respectively. It is shown that with controlling R/C ratio during the gelation process and also with control of carbonization temperature during the pyrolysis of the aerogels, carbons with controlled porosity in the range of 2nm to 15 nm can be produced.

Figure 8 shows a typical XRD spectrum of the carbon sample. The XRD spectrum indicates a broad diffraction peak located at 2θ around 23º. The peak corresponds to a plane reflection of (002) indicating a disordered structure for carbons aerogels [24]. All carbon aerogels obtained in the temperature range of 700 to 1000 ºC show the same XRD pattern which is the characteristic of an amorphous structure [25].

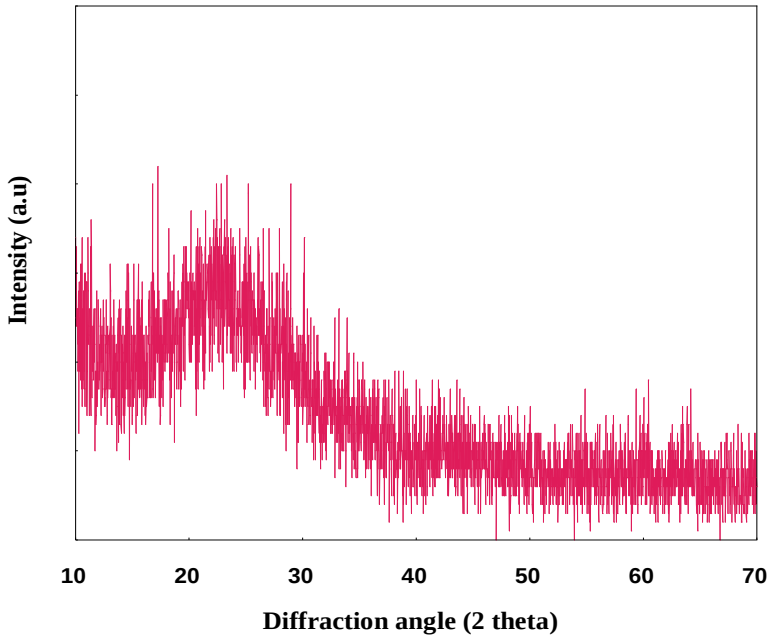

Figure 8 A typical XRD spectrum of carbon aerogel sample.

The Raman spectroscopy of the samples was also performed to further investigate the degree of crystallinity or amorphous nature of the samples. The Raman spectra of the RFC100-800 and RFC500-800 carbons are shown in Figure 9.

Both samples show a pair of distinctive broad peaks at wavelengths around 1590 cm^{-1} and 1340 cm^{-1} representing G band and D band respectively which are the characteristic peaks of carbon materials [26]. Compared with the Raman spectrum of perfect graphite which shows almost a single peak around 1575 cm^{-1} the presence of two broad peaks appeared on Raman spectra of the carbons in Figure 9 indicate an amorphous structure for carbons [27]. The ratio of the relative intensity of D band and G band (I_D/I_G) is proportional to the number of defect sites in the graphite carbon. The higher the ratio, the lower the degree of graphitization [25]. The ratio of I_D / I_G for samples RFC100-800 and RFC500-800 are 0.82 and 0.91 respectively indicating an amorphous structure for the samples which is in agreement with the XRD results. These types of materials are highly conductive due to their three dimensional cross linked internal structure.

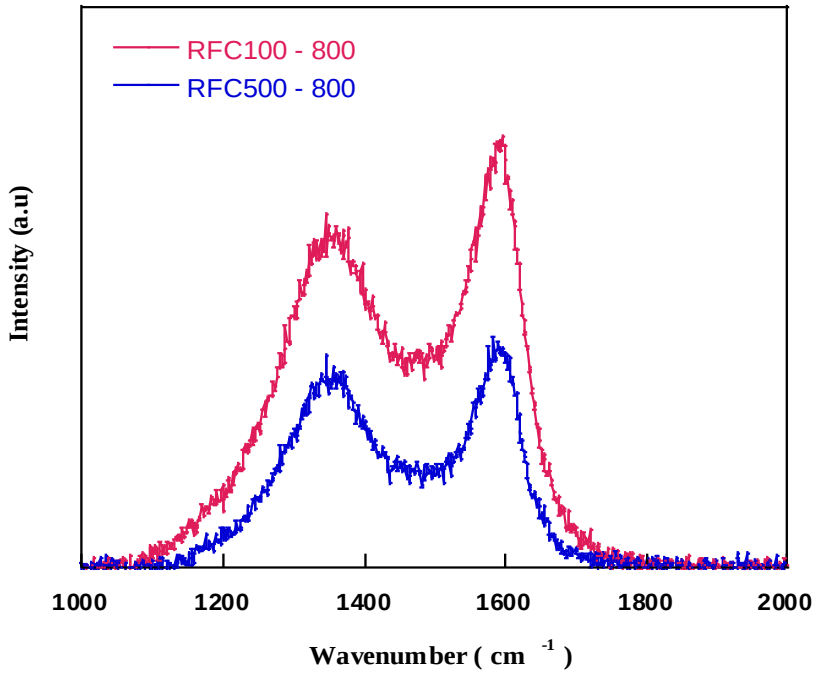

Figure 9 Raman spectra of RFC100-800 and RFC500-800 porous carbons.

Contact angle measurements

A better understanding of the wettability of the electroactive carbon materials by an electrolyte is crucial for their superior capacitance, rate capability and energy storage performance when used as an electrode for storing energy in supercapacitors. The wettability

of carbon aerogel based electrodes was investigated when 6 M KOH was used as the probing liquid for measuring the contact angles.

Appropriate surface roughness, surface energy and the type of electrolyte adopted can have a significant effect on the wettability of the surface. The wettability of a surface is determined by the outermost chemical groups of the solid. Differences in wettability between surfaces that are similar in structure are mainly due to differences in packing of the atoms [28]. It has been observed that nitrogen or oxygen modified surfaces interact with electrolyte with increased wettability due to the presence of functional groups [29]. Figure 10 shows the contact angle of electrodes prepared from carbons with different porous structure produced by the carbonization of aerogels with different R/C ratios in contact with 6 M KOH.

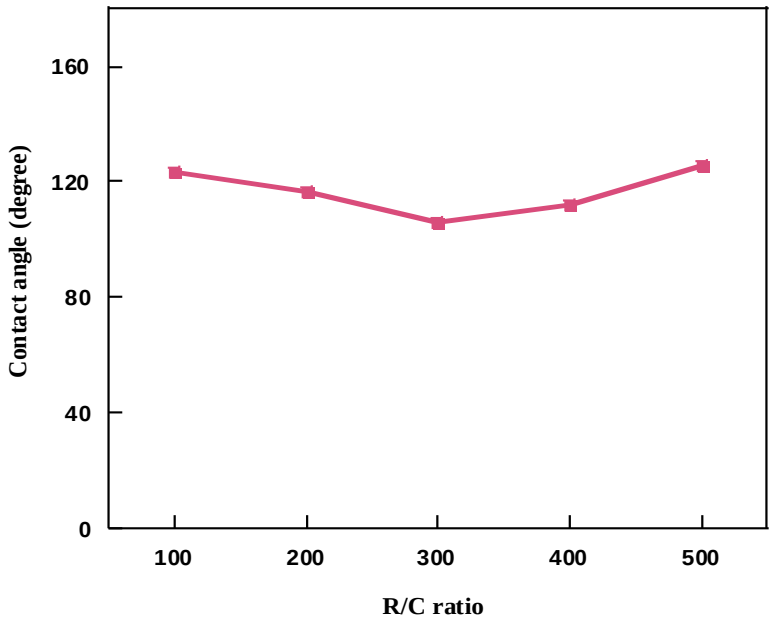

Figure 10 Contact angle measurements of carbon aerogels with different R/C ratios.

The variation of contact angles is in the range of 106º to 125º exhibiting hydrophobicity of the electrode surface since all carbons used for the electrode fabrication possess untreated surface. The electrode/electrolyte contacts can be modified by introduction of functional groups on the carbon surface.

Electrochemical analysis

Specific capacitance for the electrode was calculated by the following equation:

$$C = \frac{I}{\left(\frac{dV}{dt}\right)} \qquad (1)$$

Where *I* is the average discharge current and dV/dt is the scan rate. The specific capacitance C_{sp} in Fg^{-1} was calculated by:

$$C_{sp} = 2 \times C / m \qquad (2)$$

Where '*C*' is the measured capacitance for two-electrode cell and *m* is the mass of active material in one electrode.

Electrochemical characterisation

The specific capacitance of the carbon samples is calculated using the equations 1 and 2. It has been observed that with the increase in pore size (PS), specific capacitance (SC) was declined although the specific surface area (SSA) was increased. This can be explained using the following equation which relates the capacitance to the available surface area and the separation distance between anion and cation layers.

$$C = \frac{\varepsilon A}{d} \qquad (3)$$

Where *A* is the specific surface area, *d* is the average separation between the wall of the active material and centre of the electrolyte ion and ε is the dielectric constant.

When the pore size increases the distance between pore wall and the centre of ion is increased which results in decrease in specific capacitance [30, 31]. According to Sillars et al., the reduction in capacitance with increasing pore size could be attributed to a decrease in the dielectric constant and electrolyte conductivity, or increase in d that may occur as a result of pore flooding. Pore flooding due to excess electrolyte entering pores may cause ion pairing where the attraction of the anion to the cation is greater than the attraction to the pore wall resulting in a higher concentration of neutral ion pairs. Moreover when the pores become flooded with electrolyte the ions in the pore compete for participation in the double-layer. This may create a situation of adsorbed ions exchanging with non-adsorbed ions in the same pore impeding the formation of double layer [32]. A combination of all these will result in decrease in capacitance with increasing pore size. The lowest capacitance of 14 Fg^{-1} was obtained for the carbon with R/C ratio of 500 with larger pore size of 4.62 nm and SSA of 673 m^2g^{-1}. Results of specific capacitance of all samples along with the SSA and PS are listed in the Table 4.

To understand the effect of scan rate on the specific capacitance, the cell with electrodes using carbons with different R/C ratio as the electroactive material was tested at scan rates in

the range of 5 to 15mVs^{-1}. Typical voltammograms for the cell using a carbon with R/C ratio of 100 at different scan rates are shown in Figure 11. The highest capacitance of 136 Fg^{-1} was obtained for a cell using RFC100 carbon with average pore size of 1.80 nm as the electroactive material with the scan rate of 5mVs^{-1}. The CV loops are gradually depressed and specific capacitance decreases as the scan rate increases. This can be mainly attributed to the kinetic effects and poor ion diffusion at higher scan rates [33].

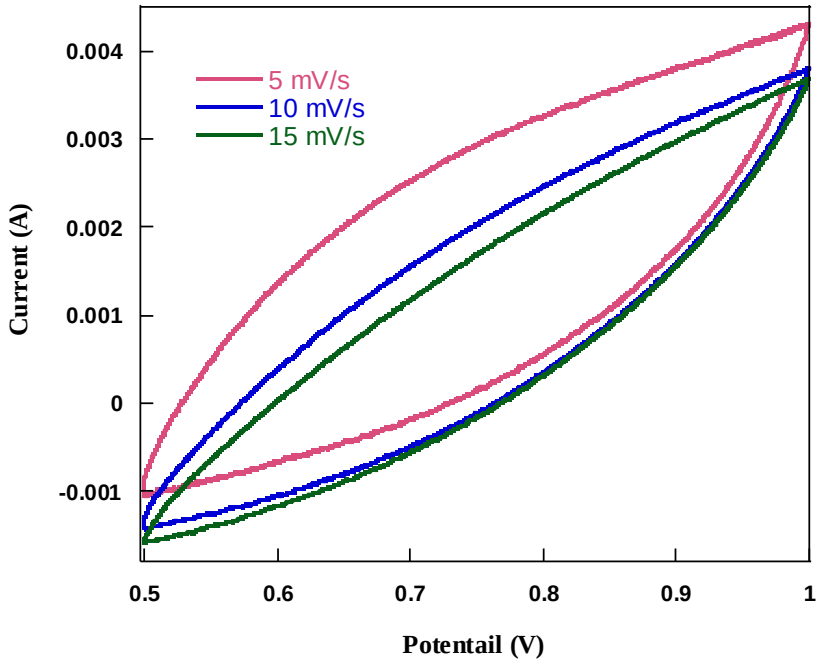

Figure 11 Cyclic voltammogram of the cell using RFC100 carbon as the electroactive material at different scan rates.

Table 4 Specific capacitance of the electrodes at different scan rate in 6M KOH electrolyte

R/C ratio	Specific surface area (m^2g^{-1})	Pore size (nm)	Specific Capacitance (Fg^{-1})		
			Scan rate (mVs^{-1})		
			5	10	15
100	537	1.80	136	71	51
200	613	2.67	109	54	29
300	633	3.08	90	40	22
400	687	3.89	81	37	25
500	673	4.62	14	8	6

Electrochemical impedance spectroscopy (EIS) is very useful technique to analyse the resistive and capacitive behaviour of the materials [34]. Figure 12 shows Nyquist plot for cell

using carbons with different R/C ratios as electroactive material in the frequency range of 100 KHz to 50 Hz.

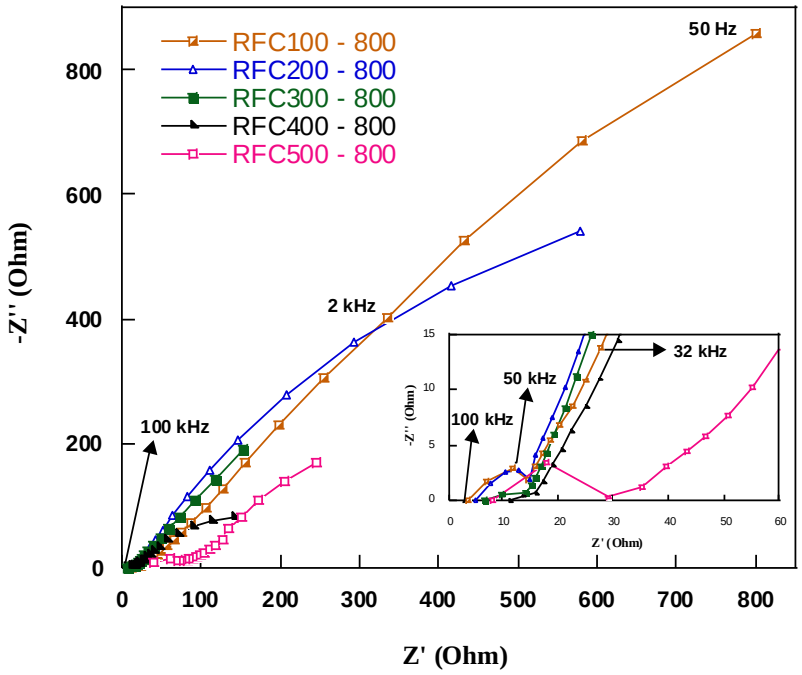

Figure 12 EIS spectra of carbon aerogels with different R/C ratios as electroactive material

The embedded graph in Figure 12 shows that at high frequencies, the imaginary part of the impedance represents resistance at the onset of the semicircle line which corresponds to the electrode/electrolyte contact and current collector series resistances. Cell behaviour at middle frequency range represents a semicircle encompassing combination of resistor and capacitor behaviour [35]. The termination of the semicircle line on the Z' axis indicates the internal resistance of the electrode. At low frequency the absence of semicircle indicates that the materials possess a low resistance and represents purely capacitive behaviour [36]. The Warburg-like behaviour of the spectra at low frequencies indicates a good ions penetration in the porous structure of the bulk electrode [29]. It can be seen that the R/C ratio affects the length; slope and position of this linear segment. A steep slope corresponding to electrodes that efficiently allow ions to penetrate pores has been observed in another study on carbon electrodes from porous carbon powder [37]. Carbon with R/C ration of 100 shows a steep line that leans more towards the vertical axis in the Warburg region. This indicates the dominance of capacitive behaviour from the formation of ionic and electronic charges of the electric double layer system at the micropore surface of the carbon at this frequency range where the ions can easily diffuse into the micropores [38-40]. With increase in the R/C ratio, the gradient of the linear part of the spectra is depressed and the length of the straight line

becomes shorter indicating the capacitive behaviour of the carbons deteriorate probably as a result of solvation effect and pore flooding of electrolyte in larger pores [32]. This indicates that in addition to the available surface area, the pore size is a key parameter controlling the capacitive behaviour of the electroactive material and final performance of the cell.

Conclusions

In this study resorcinol-formaldehyde aerogels were prepared by sol-gel polycondensation reaction. The porous structure of RF gels and carbon aerogels was controlled by changing the R/C ratio during the gel preparation and also by alteration of the carbonization temperature during the pyrolysis of the gels. Porosity analysis shows that increasing R/C ratio increases the pore size of the aerogels. The average pore size of the carbons obtained by the carbonization of the gels showed a decrease in pore size due to the shrinkage during the carbonization process. It was also observed that the carbonization process increase total pore volume and BET surface area of the samples for temperatures up to 800 ºC as a result of the release of volatile maters and opening of closed micropores. Increasing the carbonization beyond 800 ºC decreases the pore volume and surface area of the resultant carbons as a result of the collapse of their porous structure.

The resultant RF carbon aerogels were used as electroactive materials for the fabrication of electrodes. The electrodes were used in an electrochemical capacitor using 6 M KOH as electrolyte to assess the effect of their porous structure on the specific capacitance of the cell. Decrease in specific capacitance with the increase in average pore size was observed. The highest specific capacitance of 136 Fg^{-1} at the scan rate of 5 mVs^{-1} using RFC100 carbon with average pore size of 1.80 nm was achieved.

The result of EIS measurements also reveals that the carbon with R/C ration of 100 possess a good capacitive behaviour and increasing the pore size decreases the specific capacitance of the materials probably due to pore flooding by the electrolyte. This indicates that in addition to the electrode/ electrolyte contact area, the pore size is a key parameter controlling the capacitive behaviour of the electroactive material and final performance of the cell.

Acknowledgements

We would like to thank Dr Anthony Rennie in Professor Peter Hall's group at the University of Sheffield for helping with the electrochemical cell and also Dr Rizwan Raza, COMSTS institute of information technology Lahore, Pakistan for his help with Raman spectroscopy measurements.

References

1. Shabbir, I. and M. Mirzaeian, *Feasibility analysis of different cogeneration systems for a paper mill to improve its energy efficiency.* International Journal of Hydrogen Energy, 2016. **41**(37): p. 16535-16548.
2. Zhang, F., et al., *The survey of key technologies in hydrogen energy storage.* International Journal of Hydrogen Energy, 2016. **41**(33): p. 14535-14552.
3. Sawin, J.L., et al., *Renewables 2016 Global Status Report. Key findings. A Record Breaking Year for Renewable Energy: New Installations, Policy Targets, Investment and Jobs. Mainstreaming renewables: guidance for policy makers.*
4. Amrouche, S.O., et al., *Overview of energy storage in renewable energy systems.* International Journal of Hydrogen Energy, 2016. **41**(45): p. 20914-20927.
5. Cabrane, Z., M. Ouassaid, and M. Maaroufi, *Analysis and evaluation of battery-supercapacitor hybrid energy storage system for photovoltaic installation.* International Journal of Hydrogen Energy, 2016. **41**(45): p. 20897-20907.
6. Huang, G., et al., *Controllable-multichannel carbon nanofibers-based amorphous vanadium as binder-free and conductive-free electrode materials for supercapacitor.* International Journal of Hydrogen Energy, 2016. **41**(47): p. 22144-22154.
7. Wang, K., et al., *Pyrrole modified biomass derived hierarchical porous carbon as high performance symmetrical supercapacitor electrodes.* International Journal of Hydrogen Energy, 2016.
8. Ramasamy, C., J.P. del Val, and M. Anderson, *An analysis of ethylene glycol-aqueous based electrolyte system for supercapacitor applications.* Journal of Power Sources, 2014. **248**: p. 370-377.
9. Pandolfo, A. and A. Hollenkamp, *Carbon properties and their role in supercapacitors.* Journal of power sources, 2006. **157**(1): p. 11-27.
10. NAOI, K. and M. MORITA, *Advanced polymers as active materials and electrolytes for electrochemical capacitors and hybrid capacitor systems.* The Electrochemical Society Interface, 2008. **17**(1): p. 44-48.
11. Al-Muhtaseb, S.A. and J.A. Ritter, *Preparation and properties of resorcinol–formaldehyde organic and carbon gels.* Advanced Materials, 2003. **15**(2): p. 101-114.
12. Lee, Y.J., et al., *Activated carbon aerogel containing graphene as electrode material for supercapacitor.* Materials Research Bulletin, 2014. **50**: p. 240-245.
13. Mirzaeian, M. and P.J. Hall, *The control of porosity at nano scale in resorcinol formaldehyde carbon aerogels.* Journal of materials science, 2009. **44**(10): p. 2705-2713.
14. Pekala, R., *Organic aerogels from the polycondensation of resorcinol with formaldehyde.* Journal of Materials Science, 1989. **24**(9): p. 3221-3227.
15. Mirzaeian, M. and P.J. Hall, *Preparation of controlled porosity carbon aerogels for energy storage in rechargeable lithium oxygen batteries.* Electrochimica Acta, 2009. **54**(28): p. 7444-7451.
16. Lee, Y.J., et al., *Supercapacitive electrochemical performance of graphene-containing carbon aerogel prepared using polyethyleneimine-modified graphene oxide.* Current Applied Physics, 2013. **13**(5): p. 945-949.
17. Mirzaeian, M. and P.J. Hall. *Nano structure carbons for energy storage in lithium oxygen batteries*. in *Sustainable Power Generation and Supply, 2009. SUPERGEN'09. International Conference on*. 2009. IEEE.
18. Zdravkov, B., et al., *Pore classification in the characterization of porous materials: A perspective.* Open Chemistry, 2007. **5**(2): p. 385-395.
19. Ma, G., et al., *Nitrogen-doped porous carbon derived from biomass waste for high-performance supercapacitor.* Bioresource technology, 2015. **197**: p. 137-142.

20. Fiset, E., et al., *Effects of structural properties of silicon carbide-derived carbons on their electrochemical double-layer capacitance in aqueous and organic electrolytes.* Journal of Solid State Electrochemistry, 2014. **18**(3): p. 703-711.
21. Hall, P.J., et al., *Energy storage in electrochemical capacitors: designing functional materials to improve performance.* Energy & Environmental Science, 2010. **3**(9): p. 1238-1251.
22. Rouquerol, J., et al., *Adsorption by powders and porous solids: principles, methodology and applications*. 2013: Academic press.
23. Gregg, S.J., K.S.W. Sing, and H. Salzberg, *Adsorption surface area and porosity.* Journal of The Electrochemical Society, 1967. **114**(11): p. 279C-279C.
24. Sheng, J., et al., *Synthesis of microporous carbon nanofibers with high specific surface using tetraethyl orthosilicate template for supercapacitors.* International Journal of Hydrogen Energy, 2016. **41**(22): p. 9383-9393.
25. Lv, Y., et al., *A self-template synthesis of hierarchical porous carbon foams based on banana peel for supercapacitor electrodes.* Journal of Power Sources, 2012. **209**: p. 152-157.
26. Zhou, M., et al., *Nitrogen-doped porous carbons through KOH activation with superior performance in supercapacitors.* Carbon, 2014. **68**: p. 185-194.
27. Chu, P.K. and L. Li, *Characterization of amorphous and nanocrystalline carbon films.* Materials Chemistry and Physics, 2006. **96**(2): p. 253-277.
28. Mirzaeian, M., et al., *Surface characteristics of silver oxide thin film electrodes for supercapacitor applications.* Colloids and Surfaces A: Physicochemical and Engineering Aspects, 2016.
29. Candelaria, S.L., et al., *Nitrogen modification of highly porous carbon for improved supercapacitor performance.* Journal of Materials Chemistry, 2012. **22**(19): p. 9884-9889.
30. Largeot, C., et al., *Relation between the ion size and pore size for an electric double-layer capacitor.* Journal of the American Chemical Society, 2008. **130**(9): p. 2730-2731.
31. Chmiola, J., et al., *Anomalous increase in carbon capacitance at pore sizes less than 1 nanometer.* Science, 2006. **313**(5794): p. 1760-1763.
32. Sillars, F.B., et al., *Effect of activated carbon xerogel pore size on the capacitance performance of ionic liquid electrolytes.* Energy & Environmental Science, 2011. **4**(3): p. 695-706.
33. Li, J., et al., *Studies on preparation and performances of carbon aerogel electrodes for the application of supercapacitor.* Journal of Power Sources, 2006. **158**(1): p. 784-788.
34. Fernández, P., et al., *Carbon xerogels as electrochemical supercapacitors. Relation between impedance physicochemical parameters and electrochemical behaviour.* international journal of hydrogen energy, 2012. **37**(13): p. 10249-10255.
35. Ruiz, V., et al., *An activated carbon monolith as an electrode material for supercapacitors.* Carbon, 2009. **47**(1): p. 195-200.
36. Zhang, X., et al., *Fabrication of graphene and core–shell activated porous carbon-coated carbon nanotube hybrids with excellent electrochemical performance for supercapacitors.* International Journal of Hydrogen Energy, 2016. **41**(15): p. 6394-6402.
37. Chen, W.-C., T.-C. Wen, and H. Teng, *Polyaniline-deposited porous carbon electrode for supercapacitor.* Electrochimica Acta, 2003. **48**(6): p. 641-649.
38. Rafik, F., et al., *Frequency, thermal and voltage supercapacitor characterization and modeling.* Journal of power sources, 2007. **165**(2): p. 928-934.
39. Nian, Y.-R. and H. Teng, *Influence of surface oxides on the impedance behavior of carbon-based electrochemical capacitors.* Journal of Electroanalytical Chemistry, 2003. **540**: p. 119-127.
40. Gamby, J., et al., *Studies and characterisations of various activated carbons used for carbon/carbon supercapacitors.* Journal of power sources, 2001. **101**(1): p. 109-116.